Future Foods 11 (2025) 100543

Contents lists available at ScienceDirect

Future Foods

journal homepage: www.elsevier.com/locate/fufo

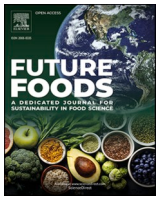

Hot or not? Modulating the functionality of artificial casein micelles with the preparation temperature

Laurens J. Antuma [a], Yuxuan Si [a], Vasil M. Garamus [b], Jan Skov Pedersen [c], Volker Gräf [d], Elke Walz [d], Remko M. Boom [a], Julia K. Keppler [a,*]

[a] Laboratory of Food Process Engineering, Wageningen University & Research, Bornse Weilanden 9, 6708 WG, Wageningen, , Netherlands
[b] Helmholtz Zentrum Hereon, Max-Planck Str. 1 21502 Geesthacht, Germany
[c] Department of Chemistry and Interdisciplinary Nanoscience Center (iNANO), Aarhus University, Gustav Wieds Vej 14 8000 Aarhus C, Denmark
[d] Max Rubner-Institut (MRI), Federal Research Institute of Nutrition and Food, Department of Food Technology and Bioprocess Engineering, Haid-und-Neu-Straße 9 76131 Karlsruhe, Germany

ARTICLE INFO

Keywords:
Re-assembled casein micelles
Recombinant casein
Cheese
Dynamic equilibrium
Process optimisation
AF4
SAXS

ABSTRACT

Identifying optimal conditions for the efficient future production of artificial casein micelles (ACM) with precision fermentation-derived caseins is essential for their application in future foods. However, casein micelles naturally form under physiological conditions with little variation, rendering it difficult to study how temperature and other factors affect their assembly. This study evaluated whether the temperature during the artificial assembly of caseins into casein micelles has a lasting impact on ACM properties and functionality. ACM were prepared at temperatures between 5 and 65 °C and stored and analysed at a fixed temperature. Micelle formation was most efficient at 37 °C, yielding the highest level of micellar casein. Casein aggregation occurred at both lower and higher temperatures, with the fraction of serum casein increasing at higher temperatures, leading to reduced micellar casein levels. Additionally, the fraction of micellar calcium phosphate and magnesium, as well as the size of calcium phosphate nanoclusters, increased with higher preparation temperatures, while micellar size and hydration decreased, resulting in denser structures. These structural and compositional changes impacted functionality, with ACM prepared at intermediate temperatures (25 and 37 °C) producing the firmest curds upon rennet coagulation, while foam stability improved for ACM prepared at lower and especially higher (65 °C) temperatures. The preparation temperature thus had irreversible effects on the ACM properties, offering a means to tailor ACM to specific applications in future foods.

1. Introduction

Casein micelles are dynamic colloids that respond to changes in their environment, including variations in temperature. Generally, casein micelles exhibit remarkable stability against heat, allowing milk to be boiled without coagulating the micelles (O'Connell and Fox, 2003). Nevertheless, temperature does affect the interactions between caseins and the solubility of calcium phosphate. At low temperatures, casein micelles swell (Nöbel et al., 2012) due to weakened hydrophobic interactions and increased solubility of calcium phosphate. This leads to the dissociation of especially β-casein (Creamer et al., 1977; Davies and Law, 1983; Rose, 1968) and partial dissolution of micellar calcium phosphate (Davies and White, 1960; Pierre and Brulé, 1981). Conversely, at increasing temperatures, caseins and ionic species migrate into the micellar phase (Liu et al., 2013; Pouliot et al., 1989a; Rose and Tessier, 1959) and the voluminosity of casein micelles decreases (Nöbel et al., 2016). These effects are almost fully reversible upon returning to the original temperature (Liu et al., 2013; Pouliot et al., 1989b). Irreversible changes occur only at higher temperatures: prolonged heating at temperatures above 100 °C causes thermal dephosphorylation, hydrolysis, and cross-linking of caseins, which ultimately leads to gelation (O'Connell and Fox, 2003).

Casein micelles naturally form in the mammalian mammary gland under physiological conditions that show little variation and cannot be controlled. Consequently, the effect of temperature and other external factors on micellar properties have been studied primarily for pre-

* Corresponding author: PO Box 17 6700 AA Wageningen, Netherlands.
E-mail addresses: laurens.antuma@wur.nl (L.J. Antuma), siyuxuan1999@gmail.com (Y. Si), vasyl.haramus@hereon.de (V.M. Garamus), jsp@chem.au.dk (J.S. Pedersen), volker.graef@mri.bund.de (V. Gräf), elke.walz@mri.bund.de (E. Walz), remko.boom@wur.nl (R.M. Boom), julia.keppler@wur.nl (J.K. Keppler).

https://doi.org/10.1016/j.fufo.2025.100543
Received 2 November 2024; Received in revised form 7 January 2025; Accepted 12 January 2025
Available online 13 January 2025

formed casein micelles, leaving the impact of these factors on the assembly process itself unclear. By contrast, the artificial assembly of caseins into so-called artificial casein micelles (ACM) allows direct control over assembly conditions such as time, pH, and temperature. ACM preparation thus provides a valuable route for studying the assembly of caseins into casein micelles at varying conditions. Additionally, precision fermentation-derived caseins may have to be assembled into ACM for application in future animal-free dairy alternatives. Therefore, investigating the effect of the assembly conditions on the properties and functionality of ACM is crucial to determine the optimal conditions for producing ACM for various food applications.

If casein micelles are in dynamic equilibrium with their surroundings (i.e. constantly exchanging caseins and ionic species), as suggested in recent casein micelle models (Holt and Carver, 2022; Horne, 2020), the conditions during the preparation of the micelles would be irrelevant for their long-term properties. Any changes brought about by variations in the preparation conditions would equilibrate towards the same state when the micelles are stored at equal conditions. However, previous studies that examined the effects of the preparation time or rate (Antuma et al., 2024a, 2024b) and pH during ACM preparation (Fan et al., 2024) suggest that the preparation conditions have lasting effects on the properties and rennet coagulation of ACM. The temperature-dependent behaviour and heat stability of ACM *after* formation have also been documented (Fan et al., 2024; Schmidt et al., 1979; Schmidt and Koops, 1977), but the impact of the temperature *during* the assembly of casein micelles on their properties and functionality remains unexplored.

In this research, we aim to study the effect of the temperature during casein micelle assembly and assess whether it can have a permanent impact on the properties and functionality of artificial casein micelles. Given the observed effect of other process parameters on ACM, we hypothesise that the preparation temperature irreversibly affects casein-casein interactions and the formation of calcium phosphate nanoclusters, thereby determining casein micelle composition (i.e. mineralisation, casein partitioning) and structure. We anticipate that these changes will, in turn, influence the functionality of the micelles, such as their rennet-induced coagulation behaviour and foaming properties. ACM are prepared from bovine sodium caseinate at various temperatures ranging from 5 °C to 65 °C and then stored and analysed at a fixed temperature. This temperature range was selected to encompass the physiological temperature of casein micelle formation (around 37 °C), as well as sufficiently lower and higher temperatures to induce significant differences in micelle assembly. The composition, internal structure, size, and hydration of the ACM are assessed, alongside their foaming and rennet coagulation behaviour. The findings from this study will deepen our understanding of casein micelle formation and establish a foundation for the precise control of ACM assembly to optimise their production for specific applications in future food products.

2. Materials and methods

2.1. Materials

Bovine sodium caseinate (Lactonat EN, 89.8 % protein, of which 41 % α_s-caseins, 44 % β-casein, and 15 % κ-casein) was kindly donated by Lactoprot (Lactoprot Deutschland GmbH, Kaltenkirchen, Germany). Calcium chloride (C1016), magnesium chloride (M8266), potassium phosphate monobasic (P5379), sodium phosphate dibasic (S7907), citric acid (C0759), potassium hydroxide (1.05033), sodium hydroxide (221465), hydrochloric acid (1.13386), nitric acid (1.00456), hydrogen peroxide (1.07209), guanidine hydrochloride (50950), l-dithiothreitol (D0632), and lactic acid solution (252476) were all purchased from Sigma-Aldrich (Merck KGaA, Darmstadt, Germany). Calcium chloride (10043–52–4) was purchased from Carl Roth (Carl Roth GmbH + Co. KG, Karlsruhe, Germany). Trifluoroacetic acid was purchased from Thermo Scientific (Thermo Fischer Scientific Inc., Waltham, MA, USA). Hydrochloric acid solution (7647–01–0) and acetonitrile ULC-MS (75–05–8) were purchased from Actu-All (Actu-All Chemicals B.V., Oss, Netherlands). Recombinantly produced chymosin (CHY-MAX Plus, batch no. 3634543) was obtained from Chr. Hansen Holding A/S (Hørsholm, Denmark). Ultrapure water (MilliQ system, Merck KGaA, Darmstadt, Germany) was used for all experiments.

2.2. Methods

2.2.1. Preparation of artificial casein micelles

ACM were prepared according to Schmidt et al. (1977) with minor adjustments. Sodium caseinate was dissolved in water at a protein concentration of 64.0 g L^{-1} by stirring at 60 °C for 30 min. Three salt solutions were prepared: solution I contained 445 mM $CaCl_2$ and 75 mM $MgCl_2$ adjusted to pH 6.70 with 0.1 M HCl, solution II contained 165 mM KH_2PO_4 and 165 mM Na_2HPO_4, and solution III contained 135 mM citrate adjusted to pH 6.70 with 1 M KOH. The caseinate solution (60 mL) and the salt solutions (10 mL each) were simultaneously pumped into a jacketed glass vessel containing a starting volume of 57 mL water over a period of 60 min. A water bath with a cooling function (CF40, JULABO Labortechnik GmbH, Seelbach, Germany) was coupled to the vessel to control the preparation temperature between 5 and 65 °C by recirculating water through the jacket of the vessel. Controlled addition of the solutions was achieved by using syringe pumps (Harvard PHD2000, Harvard Apparatus, Holliston, MA, USA and ProSense NE-1600, ProSense B.V., Oosterhout, Netherlands). During addition, the pH of the mixture was maintained at pH 6.70 with 1 M NaOH by titration (877 Titrino Plus, Metrohm AG, Barendrecht, Netherlands). After the addition of the solutions was completed, titration was continued to equilibrate the pH, during which the temperature was adjusted to 37 °C in 20 min and then maintained at that temperature for 20 min. Both during mixing and pH equilibration, the mixture was vigorously stirred by means of a magnetic stirrer. If necessary, the total volume of the solutions was brought to 150 mL with water. This yielded ACM samples with equal pH and a composition of approximately 25.6 g L^{-1} casein, 30 mM calcium, 22 mM inorganic phosphate, 5 mM magnesium, 9 mM citrate, 58 mM sodium, 40 mM potassium, and 68 mM chloride. Samples were prepared in duplicate and stored at 4 °C for at least 24 h until analysis to allow equilibration of the partitioning of ions and caseins between the micellar phase and serum phase. Samples were brought to room temperature and equilibrated at that temperature for 1.5 h before any further handling.

2.2.2. Ultracentrifugation and determination of the hydration of the pellet

ACM samples were centrifuged at 100 000 g and 20 °C for 1 h in a Beckman Coulter Optima XE-90 ultracentrifuge (Beckman Coulter Inc., Woerden, Netherlands) equipped with a 70Ti rotor. Centrifugation was conducted in duplicate. The supernatants were collected with a pipette and the supernatants of corresponding samples were combined. The apparent hydration of the pellets was determined through analysis of their moisture content according to Antuma et al. (2023).

2.2.3. Analysis of ion partitioning

The cationic content (calcium, phosphorus, magnesium, sodium, and potassium) of ACM samples and their ultracentrifugal supernatants was analysed by inductively coupled plasma optical emission spectrometry (ICP-OES). First, samples were prepared by microwave-assisted wet digestion. Approximately 0.5 mL solution was mixed with 10 mL aqua regia (7.5 mL HCl + 2.5 mL HNO_3) and 1 mL H_2O_2. Subsequently, the mixture was subjected to a temperature program in an ETHOS EASY microwave digestion system (Milestone Srl, Sorisole, Italy) according to Guimarães et al. (2021). The digested material was collected in volumetric flasks. The digestion flasks were rinsed with water and the rinse water was also transferred to the volumetric flasks. The digest was then diluted to a total volume of 100 mL with water. Samples were prepared in duplicate and analysed in triplicate with the operational conditions as

specified in Guimarães et al. (2021). Elements were detected in radial view, unless stated otherwise, at the following wavelengths: Ca 393.366 nm, P 178.221 nm (axial), Mg 279.553 nm, Na 589.592 nm, K 766.490 nm.

The anionic content (chloride, phosphate, and citrate) of ACM samples and their ultracentrifugal supernatants was analysed by ion chromatography (IC). ACM samples were diluted 500-fold and supernatants were diluted 200-fold in water. Solutions were then analysed on a Dionex ICS-6000 liquid chromatography system equipped with a 2 mm standard bore Dionex IonPac AS17-C column for anion analysis (Thermo Fisher Scientific B.V., Breda, Netherlands) at 30 °C with a flow rate of 0.25 mL min^{-1} and injection volume of 5 μL. Gradient elution was conducted with KOH, first set to 5 mM for 10 min, followed by a linear increase to 40 mM within 15 min, an isocratic elution at 40 mM for 6 min, and a linear decrease to 5 mM in 5 min. A conductivity detector was used for peak detection. Samples were analysed in duplicate.

Concentrations of ionic species in the supernatants were corrected for the excluded volume with a correction factor K calculated according to Pierre and Brulé (1981):

$$K = \frac{1000 - P(1 + W)}{1000} \quad (1)$$

where P is the measured micellar protein content in g L^{-1} and W is the measured apparent hydration of the micellar phase in g water g^{-1} dry matter. The micellar concentration of the ionic species was then calculated as the difference between the total concentration and the corrected supernatant concentration.

2.2.4. Quantification of casein aggregation

The prepared ACM were diluted 20-fold in simulated milk ultrafiltrate (SMUF) prepared according to Dumpler et al. (2017) and the aggregated particles were then removed by vacuum filtration. Cotton filters (ϕ = 90 mm) with a particle retention of 20 μm (Whatman™ Grade 41, Cytiva, Global Life Sciences Solutions USA LLC, Marlborough, MA, USA) were weighed, placed in a Büchner funnel, and wetted with approximately 100 mL SMUF, after which the diluted samples were applied. A vacuum pump (SC950, KNF Neuberger GmbH, Freiburg, Germany) was coupled to a Büchner flask and used to apply the driving force for filtration. The power level was set to 20 %. Filtration was continued until 1 L liquid was filtered or until the filter was clogged. The filters were carefully removed and placed in pre-weighed aluminium pans (ϕ = 100 mm) and dried at 105 °C for approximately 48 h in a hot air oven (Binder model E 28, Binder GmbH, Tuttlingen, Germany). Additionally, filters through which only 1 L SMUF was filtered were dried to serve as a blank. Filtrations were conducted in duplicate. The amount of retentate was determined by calculating the difference in weight of the filters before filtration and after drying and subtracting the difference in weight of the blank filters from that. It was assumed that the retentate consisted solely of casein. The fraction of aggregated casein was then calculated by dividing the weight of the retentate by the total weight of casein in the volume of liquid that was filtered.

2.2.5. Analysis of casein partitioning

ACM samples were diluted 6-fold and supernatants were diluted 3-fold in a buffer solution of 6 M guanidine hydrochloride, 20 mM dithiothreitol, and 5 mM sodium citrate. Their casein content and composition were then determined by high-performance liquid chromatography (HPLC) as described in Antuma et al. (2024b). Micellar casein was calculated as the total casein minus the aggregated casein and supernatant casein.

2.2.6. Internal structure analysis

Small-angle X-ray scattering (SAXS) measurements were performed at Helmholz-Zentrum Hereon (Geesthacht, Germany) with a laboratory SAXS instrument (Xeuss 3.0, Xenocs SAS, Grenoble, France) according to Antuma et al. (2023). Measurements were performed in duplicate to check the reproducibility of the preparation procedure. The main characteristics of the used equipment are a GeniX 3D μ-source X-ray beam delivery system emitting the wavelength of the Cu-Kα line and a Pilatus3 R 300 K detector (Dectris AG, Baden-Daettwil, Switzerland, pixel size 172×172 μm^2). The length of the collimation line was 181.5 cm, and the sample-to-detector distance was 90 cm (the accessible q-range ranged from 0.004 to 0.330 $Å^{-1}$). The beam size on the sample was 0.5 mm and the acquisition time was 4000 s. Samples were filled into borosilicate glass capillaries of 1.5 mm in diameter (B-15–001–80, WJM-Glas/Müller GmbH, Berlin, Germany). Data collection was performed at room temperature. The raw scattering data were corrected for the background from the solvent (SMUF) measured in a capillary with the same diameter and instrumental noise. Isotropic 2D data were azimuthally integrated to obtain I(q)-scattering intensities versus q and converted to absolute units using the standard procedure of Xeuss 3.0 (automatic measurement of transmitted beam and definition of region of interest of transmitted beam).

To extract information on the internal structural variations of the ACM, modelling of the scattering data was performed using the model of Pedersen et al. (2022). On the shortest length scales, it includes both colloidal calcium phosphate nanoclusters (CCPs) and protein moieties, which are described as, respectively, ellipsoidal particles and star-like structures. Correlations between these structures are taken into account using partial structure factors. The model describes the overall scattering as originating from polydisperse spheres and, additionally, a contribution from intermediate length scale variations (sometimes termed incompressible regions). An inter-micelle structure factor is included in the local monodisperse approximation to account for concentration effects (Pedersen, 1994). The SAXS data were fitted on an absolute scale using scattering length densities and concentration of the components as restraints. The data at the lowest q are influenced by instrumental smearing and therefore the model intensity was smeared by an instrumental resolution function that takes these effects into account (Barker and Pedersen, 1995; Pedersen et al., 1990). Model parameters were optimised using standard least-squares methods (Pedersen, 1997).

The SAXS data did not cover sufficiently low q to allow the overall size and polydispersity to be fitted. The values were therefore taken from dynamic light scattering analysis and fixed at these values. Furthermore, the effective hard-sphere volume fraction $\eta_{HS,mic}$ is the structure factor describing micelle concentration effects and was fixed at 0.07, which is reasonable for the concentration of the components and the expected hydration of the structures. The CCP-CCP correlations were not directly observed in the SAXS data and therefore the parameters related to the structure factor were fixed at the values estimated for native casein micelles (Pedersen et al., 2022). For the protein star-like clusters, the length of the arms, L_{prot}, in the protein star-like clusters was fixed at 44 Å, their radius, R_{prot}, was fixed at 7 Å, and the number of arms, n_{arms}, was fixed at 6. Furthermore, the expansion factor of the CCPs, which reflects the hydration of these particles, was fixed at 1.5, a value which agrees with that of bovine casein micelles (Pedersen et al., 2022).

The parameters optimised in the fit to the SAXS data were the average size and number of intermediate structures, R_{int} (relative polydispersity σ_{int} fixed at 0.7) and n_{int}, the radius and axis ratio of CCPs, R_{CCP} and ϵ, the effective volume fraction and interaction radius related to the CCP-protein and protein-protein correlations, η_{HS} and R_{HS}, the total number of CCPs and protein clusters in a micelle, n_{sub}, and mass of the protein clusters, M_{prot}. Note that the values n_{sub} as well as the value for the calculated total mass of a micelle are mainly given by the values of the average size and the related polydispersity as derived from dynamic light scattering. An overview of the parameters used in the model and their physical meaning is given in Table 1.

Table 1
Parameters included in the model used to fit the SAXS data, including their description and physical meaning.

Parameter	Description	Physical meaning
R_{mic} (Å)	Overall number-average radius of casein micelles	Overall size of micelles when described as spherical object
σ_{mic} (-)	Relative polydispersity of the overall micelle radii	Spread in overall size
$\eta_{HS,mic}$ (-)	Volume fraction of casein micelles	Part of the volume of the system that the micelles take up including their internal hydrating water
R_{int} (Å)	Number-average radius of the intermediate structures	Size of internal fluctuations on length scales below the overall micelle size and above that of the substructures of proteins and calcium phosphate clusters. These structures are also described as being spherical.
σ_{int} (-)	Relative polydispersity of the intermediate structures	Spread in the size of the intermediate fluctuations
n_{int} (-)	Ratio of the overall forward scattering to that of the intermediate structures	Related to the influence of the intermediate fluctuations relative to the total micelle. When low, the importance is most pronounced.
l_{prot} (Å)	Contour length of the arms in the polymer star structure	Protein local structure is described as particle-like, i.e. as star structures with six straight arms
$n_{arm,prot}$ (-)	Number of arms of the proteins	Number of arms in the model for the local protein structures
R_{CCP} (Å)	Radius of the oblate ellipsoidal calcium phosphate nanoclusters	Radius of the calcium phosphate nanoclusters, which are described as ellipsoids of revolution
ϵ (-)	Axis ratio of calcium phosphate nanoclusters	Axis ratio of the ellipsoids describing the calcium phosphate clusters
n_{sub} (-)	Ratio of the forward scattering to the level of the scattering of the substructures	Number of protein particles and calcium phosphate clusters in a micelle
$\eta_{HS,sub}$ (-)	Volume fraction of the substructures	Protein and calcium phosphate particles are correlated in the packing inside the micelle. This is described by an effective hard-sphere structure factor, and this is the effective volume fraction that enters the structure factor.
$R_{HS,sub}$ (-)	Hard-sphere interaction radius of the substructures	Effective interaction radius of the protein and calcium phosphate particles when described by the effective hard-sphere structure factor
R_{prot} (Å)	Radius of protein particles	Radius of the single protein strands in the star structure that describes the local protein structure
M_{prot} (Da)	Molar mass of the protein heterogeneities	Molar mass of the local protein structures
C_{mic} (g L^{-1})	Concentration of casein micelles	Overall concentration of micelles including proteins and calcium phosphate nanoclusters
$f_{mass,prot}$ (-)	Mass fraction of protein	The fraction of the micelle that is made up of protein
M_{tot} (MDa)	Total molar mass of the casein micelles	Total mass of casein micelle

2.2.7. Particle size analysis

Samples were diluted 100-fold in 10 mM $CaCl_2$ in water and filtered with glass fibre syringe filters (7–8808, neoLab Migge GmbH, Heidelberg, Germany) with a pore size of 1.2 μm, after which the size and polydispersity of the ACM were analysed with dynamic light scattering by using a Malvern Zetasizer Nano ZS (Malvern Panalytical Ltd, Worcestershire, UK). The device was equipped with a He-Ne laser with a wavelength of 633 nm. The refractive index of the dispersion medium was set at 1.33, its viscosity at 0.8872 mPa s, the real part of the refractive index of the casein micelles at 1.57 (Griffin and Griffin, 1985), and their absorption at 0.001. Samples were first brought to room temperature and then equilibrated at 25 °C for 120 s inside the device before analysis. Measurements were carried out at 25 °C with a fixed scattering angle of 173°. Each measurement consisted of 3 sub-measurements, each of which consisted of a minimum number of 12 runs controlled by the software (version 8.01.4906). The harmonic intensity-weighted average hydrodynamic diameter (referred to as Z-average) and polydispersity index provided by the software were calculated by cumulant analysis using the general-purpose model.

2.2.8. Asymmetrical flow field-flow fractionation

Samples were diluted 100-fold in 10 mM $CaCl_2$ in water and filtered with glass fibre syringe filters (7–8808, neoLab Migge GmbH, Heidelberg, Germany) with a pore size of 1.2 μm. Asymmetrical flow field-flow fractionation (AF4) analysis was performed on an AF2000 MT Aqueous system (Postnova Analytics GmbH, Landsberg am Lech, Germany). This is a separation technique used to analyse nanoparticles, vesicles, and macromolecules such as proteins and polymers. Separation occurs in a flat channel without a solid matrix, thereby excluding potential interactions with a stationary phase, such as in HPLC analysis. The porous bottom of the channel is covered with a membrane, allowing the liquid to permeate while preventing particles from passing through (depending on the pore size of the membrane). The separation process is based on a crossflow perpendicular to the detector flow, which transports the sample through the channel. The crossflow guides the particles towards the channel wall with the membrane. Due to their size-dependent Brownian motion, smaller particles diffuse more quickly against the crossflow into regions of higher flow velocity in the centre of the channel. Thereby, smaller particles elute earlier and reach the detectors sooner than larger particles. Detection of the particles can then be achieved by using a combination of detectors.

The AF4 system was coupled to a PN8050 fraction collector, a PN3621 multi-angle light scattering (MALS) detector operating at a wavelength of 532 nm, and a PN3241 UV/VIS diode array detector. A PN1130 isocratic pump with an in-line vacuum degasser (PN7520) generated the carrier flow. Samples were injected into the channel by an autosampler (PN5300). The analytical channel was fitted with a spacer of 350 μm in thickness and a 10 kDa regenerated cellulose membrane. The carrier liquid consisted of 10 mM $CaCl_2$ in water and was filtered (Omnipore™ 0.1 μm PTFE, Merck KGaA, Darmstadt, Germany) before use. A detector flow rate of 0.5 mL min^{-1} was used and the injection volume was 100 μL. After a 2 min delay time, a 4 min focusing step was performed at a cross-flow rate of 0.8 mL min^{-1} and an injection flow rate of 0.2 mL min^{-1}. The focus flow opposes the detector flow and prevents immediate elution and uncontrolled distribution of the particles throughout the channel. The elution step consisted of a constant flow rate of 0.8 mL min^{-1} for 10 min, followed by an exponentially decreasing flow rate (exponent = 0.2) to 0.1 mL min^{-1} in 15 min and a subsequent linear decrease from 0.1 mL min^{-1} to 0 mL min^{-1} in 40 min. The cross-flow rate was then maintained at zero for 5 min. Similar procedures have been reported by Glantz et al. (2010) and Lie-Piang et al. (2021).

Data collection and evaluation were performed with NovaFFF AF2000 (version 2.2.0.1) and LabSolutions Postrun Analysis (version 5.97 SP 1) software. Radii of gyration were calculated from a first-order fitting of the MALS data by using the Berry model (Abbate et al., 2019). Scattered light signals from the angles between 36° and 140° (15 angles) were used for these calculations and detectors at the lowest and highest angles were excluded because of the high noise.

2.2.9. Monitoring of chymosin-induced coagulation behaviour

The pH of ACM samples was adjusted to 6.3 by means of acidification below 10 °C with an 8.5 % lactic acid solution in water. Samples were left to equilibrate overnight at 4 °C, after which the pH was readjusted to 6.3 before analysis. Subsequently, 0.04 % (v/w) calcium chloride was added by means of a 4 % (w/v) calcium chloride solution and the samples were heated to 30 °C while stirring. Samples were then renneted

by adding 0.02 % (v/w) chymosin by means of a solution of 10-fold diluted chymosin in water. Coagulation was monitored for 60 min through oscillatory rheometry according to Antuma et al. (2024a). The coagulation time was taken as the time at which the storage modulus exceeded 2 Pa. Samples were analysed in duplicate.

2.2.10. Analysis of foaming capacity

The foaming properties of ACM samples were assessed by analysis with a Foamscan™ foam analyser (TECLIS Instruments, Civrieux d'Azergues, France) as described by Hoppenreijs et al. (2024). ACM samples were injected stepwise into the glass cylindrical column of the Foamscan to calibrate the conductivity sensor. Initially, 16 mL (1 mL to fill the dead volume in the injection tube and the remaining 15 mL to fill the column) was injected by using a syringe, followed by three additions of 5 mL each. Foams were produced by sparging the 30 mL aliquots with compressed air at a rate of 300 mL min^{-1} through a glass frit with a pore size of 16–20 μm (P3, TECLIS Instruments). Sparging was continued until a foam volume of 160 mL was achieved. The decay of the foam volume over time was monitored by the built-in camera of the system. The half-life time of the foam was determined as the time taken for the foam to collapse to half of its original volume. The column temperature was maintained at 20 °C by using a water bath that recirculated water through the column jacket. Each sample was measured in triplicate.

2.2.11. Data analysis and presentation

Descriptive statistics were computed with Microsoft Excel 365 (version 2208). Graphs were created with OriginPro (version 2022, OriginLab Corporation, Northampton, MA, USA). Unless otherwise specified, results are expressed as the mean ± standard deviation of independent duplicates. Technical replicates were averaged before calculating the standard deviation.

4. Results

The impact of the preparation temperature on the level of colloidal calcium phosphate was quantified (Fig. 1). The colloidal fraction of calcium was stable at around 71.7 % of the total calcium when the preparation temperature of the ACM increased from 5 to 37 °C and increased by 1.8 % when the preparation temperature was further increased to 65 °C. Similarly, the colloidal fraction of inorganic phosphate hovered around 52.2 % of the total for ACM prepared between 5 and 37 °C, which then increased to 55.9 ± 1.4 % when the preparation temperature was increased to 65 °C. The colloidal fraction of magnesium showed a linear increase from 36.2 ± 1.2 to 43.2 ± 0.6 % with the preparation temperature (Fig. 1). No clear trend was observed in the partitioning of citrate between the colloidal phase and the serum.

The partitioning of caseins between the colloidal phase and serum phase was also analysed. ACM were pelleted by ultracentrifugation and the fraction of the caseins in the serum phase was quantified. This fraction of serum casein was constant at about 5 % of the total casein at preparation temperatures between 5 °C and 37 °C and then increased to 13.7 ± 0.4 % for ACM prepared at 65 °C (Fig. 2). β-Casein and κ-casein were mainly responsible for these increases, with the fraction of the total β-casein in the serum increasing from 9 % to 20 % and the fraction of the total κ-casein from 7 % to 27 % (data not shown).

The fraction of micellar casein is commonly assumed to constitute the pelleted caseins (i.e. the total casein minus the serum casein). However, casein aggregation into larger aggregates was visually observed in part of the mixtures and these aggregates would sediment with the ACM upon ultracentrifugation. Analysis by laser diffraction

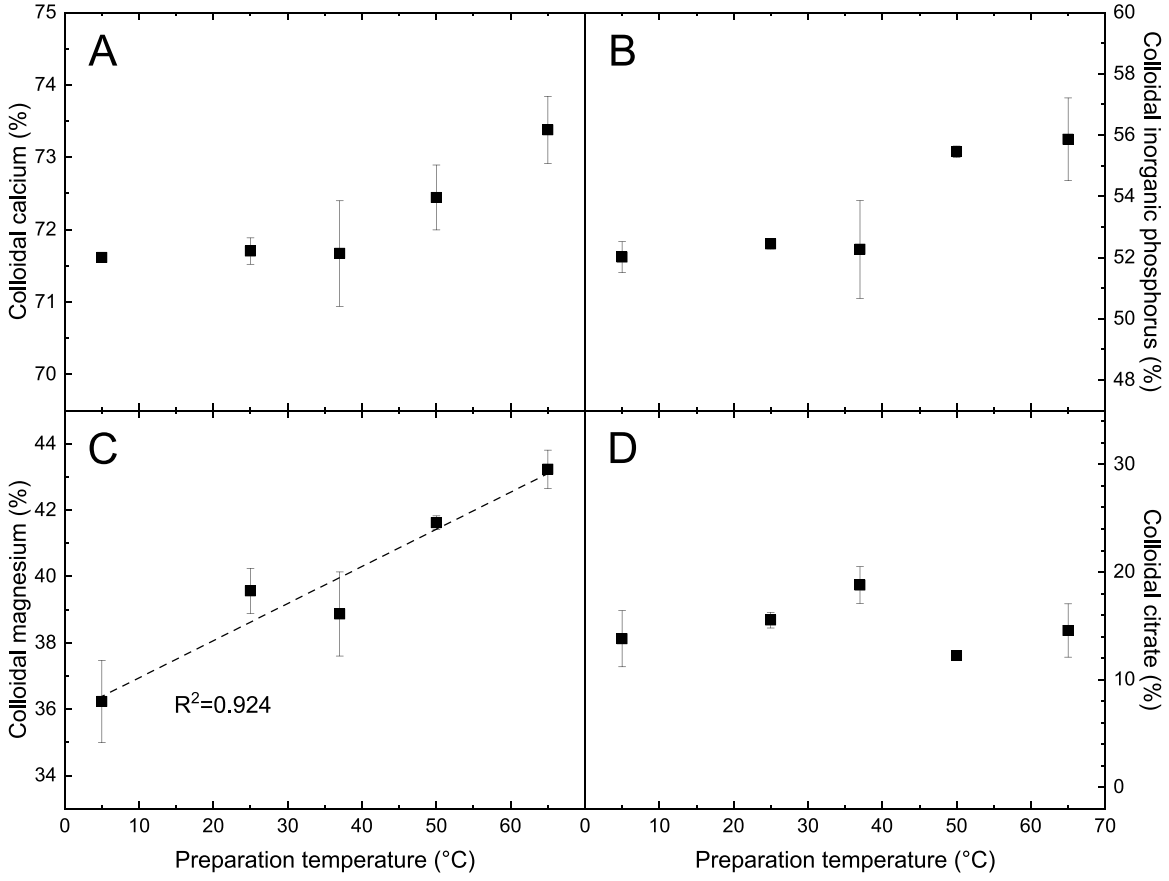

Fig. 1. Colloidal (A) calcium, (B) inorganic phosphorus, (C) magnesium, and (D) citrate as a percentage of their total concentrations for ACM prepared at various temperatures.

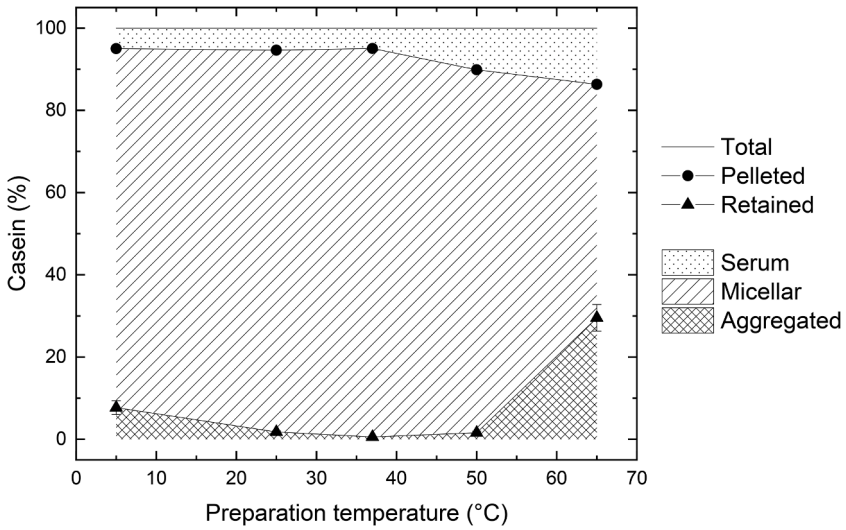

Fig. 2. The total level of casein and the levels of casein pelleted upon ultracentrifugation and retained upon filtration as percentages of the total casein in ACM prepared at various temperatures. The level of serum casein is represented by the area between the total casein and pelleted casein, the level of micellar casein by that between the pelleted casein and retained casein, and the level of aggregated casein by that below the retained casein. Error bars are depicted but are smaller than the symbols in most cases.

indicated that these aggregates were larger than 20 μm in diameter (data not shown). The extent of aggregation was therefore quantified by filtering the ACM through filters with a nominal particle retention of 20 μm and analysing the retentate weight. Almost no casein aggregation was observed in ACM prepared at 37 °C (0.6 ± 0.1 % of the total casein), but gradually more casein aggregated at higher or lower preparation temperatures (Fig. 2). For ACM prepared at 5 °C, 7.7 ± 1.7 % of the total casein was present in aggregates, while this was 29.6 ± 3.2 % for those prepared at 65 °C.

The fraction of micellar casein was finally calculated by subtracting the fraction of aggregated casein and serum casein from the total casein. ACM prepared at 37 °C exhibited the highest fraction of micellar casein at 94.5 ± 0.1 % (Fig. 2). As a result of the casein aggregation, a temperature of 5 °C during ACM preparation resulted in a smaller fraction of micellar casein of 87.3 ± 0.1 %. The increased level of serum casein in combination with more casein aggregation at higher temperatures resulted in considerably smaller fractions of micellar casein. For ACM prepared at 65 °C, the fraction of micellar casein was reduced to 56.8 ± 0.4 % of the total casein (Fig. 2).

The hydrodynamic diameter of the ACM was determined by dynamic light scattering analysis, as well as AF4 analysis. Dynamic light scattering results showed that the diameter of ACM slightly decreased from 154.3 ± 4.9 to 140.7 ± 1.1 nm when the preparation temperature of the ACM was increased from 5 to 65 °C (Fig. 3A). ACM prepared at 37 °C diverged from this trend with a larger diameter of 167.1 ± 1.2 nm. The polydispersity index was relatively constant at around 0.17 for all preparations (not depicted). AF4 analysis was conducted to obtain more information about the size distributions and the typical curves obtained are shown in Fig. 3B. All ACM dispersions exhibited a single size population with an approximate range of 25–125 nm in radius. The radius of gyration (R_g) at the elution time at which the intensity of the MALS signal shows a peak (i.e. the mode of the micelle radius; Table 2) aligned

Table 2
Elution time and radius of gyration (R_g) at the maximum peak height of the MALS signal intensity for ACM prepared at various temperatures.

Preparation temperature (°C)	Elution time at maximum peak height (min)	R_g at maximum peak height (nm)
5	29.0 ± 0.3	78.0 ± 3.0
25	28.8 ± 0.2	75.2 ± 4.5
37	29.9 ± 0.0	81.6 ± 0.0
50	27.8 ± 0.6	66.2 ± 7.8
65	27.1 ± 2.1	60.9 ± 12.9

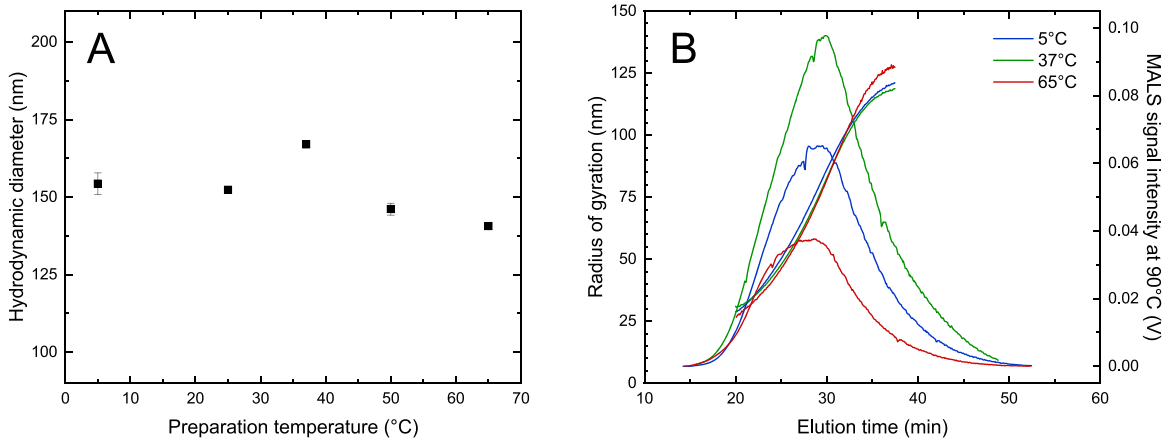

Fig. 3. (A) Hydrodynamic diameter and (B) radius of gyration (rising curves) and MALS signal (peaks) versus elution time in AF4 experiments of ACM prepared at various temperatures.

well with the measured average hydrodynamic diameters. The same trend was observed for the mode of the radii of gyration as for the average hydrodynamic radius (R_h), with an overall decrease when the preparation temperature of the ACM increased and a peak at a preparation temperature of 37 °C.

The internal structure of the ACM was investigated with SAXS (Fig. 4A). The scattering curves of the ACM prepared at 5 and 25 °C overlap at intermediate q-range, whereas they deviate slightly at low q and high q. The latter deviation is probably due to a slight mismatch in the subtraction of the background. The scattering signal of ACM prepared at 37 °C overlaps well with that of the ACM prepared at the two lower temperatures at high q (0.08–0.30 $Å^{-1}$), whereas the intensity was lower in the region of 0.01 to 0.08 $Å^{-1}$ where the intermediate structures and the sub-particles contribute to the scattering. The signals of the ACM prepared at 50 and 65 °C were higher in the middle range (0.025–0.10 $Å^{-1}$) than for the ACM prepared at lower temperatures. However, the shoulders at 0.08 $Å^{-1}$, which are influenced by the sub-particle size and the correlations between them, are less pronounced. This suggests that some of the particles were larger and less correlated when the ACM were prepared at increased temperatures.

For further insight into the overall and internal structure of the micelles, the SAXS data were fitted by the model described in Section 2.2.6. This model describes the micelles as polydisperse spheres consisting of protein moieties and calcium phosphate nanoclusters that are correlated due to their relatively dense packing and are somewhat inhomogeneously distributed on intermediate length scales (Pedersen et al., 2022). This model is appropriate due to the close resemblance of the obtained SAXS scattering curves with those of native casein micelles. The fits are displayed in Fig. 4B and the results are shown in Table 3, which also contains information from the dynamic light scattering analysis (R_{mic} and σ_{mic}) as well as the micellar concentration of casein and calcium phosphate and the calculated overall number-average mass of the particles (M_{tot}). The modelling shows that the CCPs increased slightly in size with the preparation temperature, whereas there was a pronounced increase in the mass of the protein moieties, which increased from about 60 kDa at 5 °C to 100 kDa at 65 °C, reflecting a significantly larger impact of preparation temperature on the protein state than on the CCPs. These variations are robust results since the fits converged to this also when different initial values were used.

The local dense packing of CCPs and protein moieties requires the use of an effective hard-sphere structure factor in the model (Pedersen et al. 2022). The fits revealed that the parameter related to CCP-protein and CCP-CCP correlations (the interaction radius $R_{HS,sub}$) increased at the two highest temperatures, whereas the effective volume fraction

Table 3
Results from fitting the scattering from ACM prepared at different temperatures as shown in Figure 4B. Parameters marked by a star were fixed in the fit.

Parameter	Preparation temperature (°C)				
	5	25	37	50	65
R_{mic} (Å)	784*	840*	840*	762*	724*
σ_{mic} (-)	0.417*	0.417*	0.423*	0.407*	0.398*
$\eta_{HS,mic}$ (-)	0.070*	0.070*	0.070*	0.070*	0.070*
R_{int} (Å)	98 ± 1	71 ± 2	87 ± 2	64 ± 1	70 ± 1
σ_{int} (-)	0.700*	0.700*	0.700*	0.700*	0.700*
n_{int} (-)	155 ± 10	1219 ± 100	849 ± 70	950 ± 55	710 ± 60
l_{prot} (Å)	44*	44*	44*	44*	44*
$n_{arm,prot}$ (-)	6*	6*	6*	6*	6*
R_{CCP} (Å)	21 ± 1	23 ± 2	23 ± 1	25 ± 2	28 ± 3
ϵ (-)	0.69 ± 0.14	0.49 ± 0.10	0.52 ± 0.08	0.56 ± 0.11	0.49 ± 0.14
n_{sub} (-)	104600 ± 2500	186300 ± 3000	216100 ± 3200	141000 ± 1800	895001 ± 1500
$\eta_{HS,sub}$ (-)	0.057 ± 0.005	0.065 ± 0.009	0.054 ± 0.006	0.045 ± 0.011	0.025 ± 0.018
$R_{HS,sub}$ (-)	37.6 ± 1.3	39.7 ± 2.0	37.5 ± 1.8	45.6 ± 2.8	48.8 ± 7.1
R_{prot} (Å)	7.0*	7.0*	7.0*	7.0*	7.0*
M_{prot} (Da)	57900 ± 2373	41000 ± 4100	41100 ± 2800	75300 ± 3200	103000 ± 5600
C_{mic} (g L^{-1})	23.4*	25.7*	26.9*	24.1*	16.7*
$f_{mass,prot}$ (-)	0.907*	0.911*	0.913*	0.908*	0.901*
M_{tot} (MDa)	6.05	7.63	8.89	10.70	9.22

$\eta_{HS,sub}$ decreased. This is likely a result of the increased size of the protein moieties and their simultaneously lower correlation (i.e. less well-defined distance between them) in ACM prepared at higher temperatures. This agrees with the expectation that high temperature can lead to protein aggregation and a locally more disordered structure (Moitzi et al., 2008). The parameter n_{int} reflects the ratio between the forward scattering of the whole particles and that of the intermediate structures. When this parameter is low, the intermediate structures contribute more to the scattering than when it is large, meaning that a lower value represents increased heterogeneity. Considering this, ACM prepared at 5 °C were the most heterogeneous.

The hydration of the micelles was determined by centrifugation and analysis of the moisture content of the pellet. In samples without casein micelle aggregates, this yields the apparent hydration of casein micelles. However, partial aggregation of casein micelles was observed in ACM samples prepared at low and high temperatures (Fig. 2). These aggregates are also sedimented upon centrifugation and are therefore

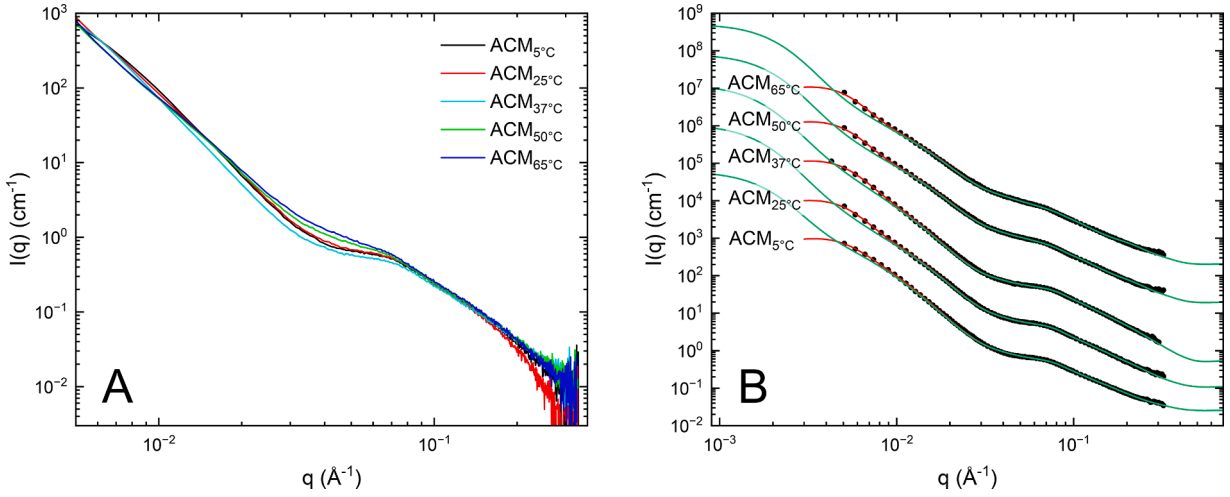

Fig. 4. (A) SAXS scattering intensities of ACM prepared at different temperatures and (B) the same signals (shifted; increasing preparation temperature from bottom to top) with fits. The ideal, non-smeared fit to the data is represented by the green curves and the red curves include instrumental smearing.

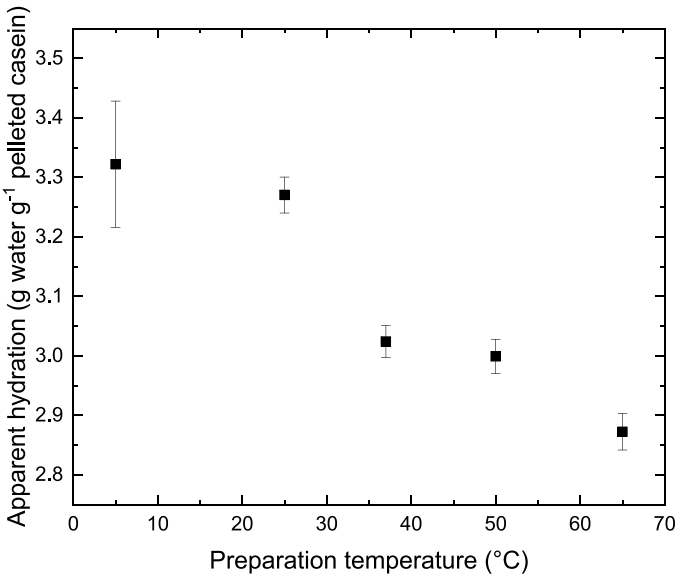

Fig. 5. Apparent hydration of ACM prepared at various temperatures.

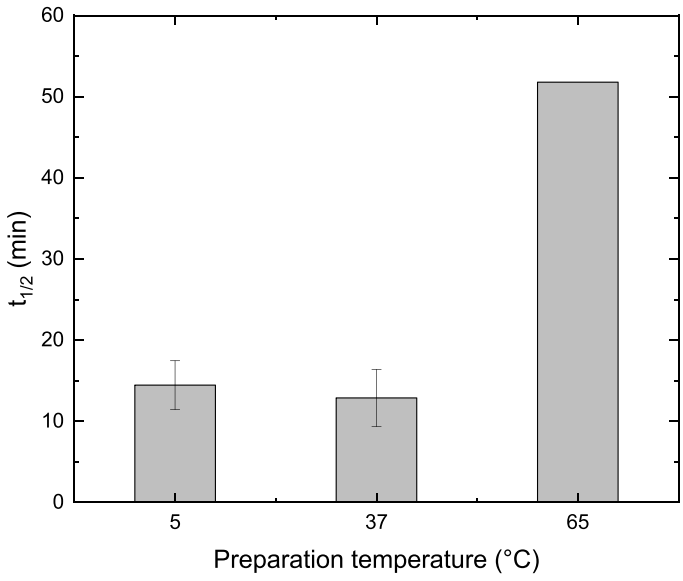

Fig. 7. Half-life time ($t_{1/2}$) of foams stabilised by ACM prepared at various temperatures.

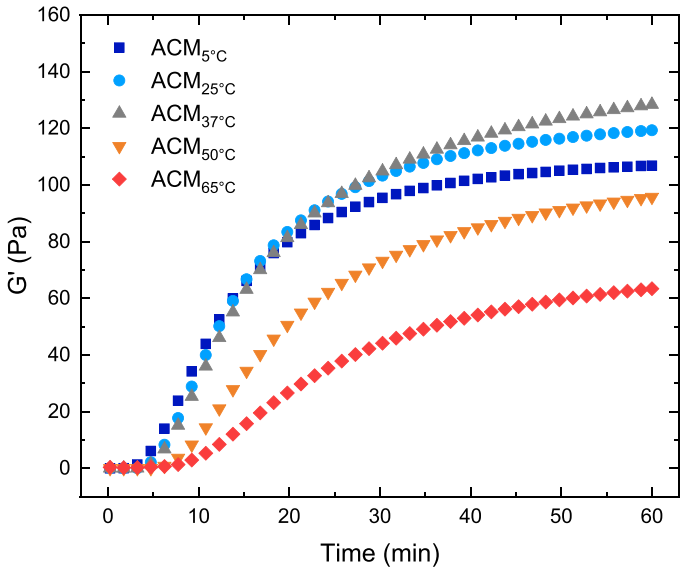

Fig. 6. Development of the storage modulus G' over time of ACM prepared at various temperatures during incubation at a fixed temperature of 30 °C with chymosin.

included in the values of the apparent hydration. This apparent hydration of the pelleted casein decreased from 3.32 ± 0.11 to 2.87 ± 0.03 g water g^{-1} pelleted casein as the preparation temperature increased from 5 to 65 °C (Fig. 5).

The ACM were coagulated at a fixed temperature of 30 °C by the enzymatic action of chymosin and the coagulation behaviour was monitored over time by rheometry. The results are shown in Fig. 6. The coagulation time (i.e. time until the onset of coagulation) of the ACM was consistent at preparation temperatures between 5 and 37 °C and increased as the preparation temperature of the ACM increased to 65 °C. The maximum storage modulus of gels increased from 106.9 ± 1.3 to 128.4 ± 0.9 Pa when the preparation temperature of the ACM increased from 5 to 37 °C, followed by a decrease to 63.4 ± 1.3 Pa when it was further increased to 65 °C.

In addition to the coagulation properties, the foaming properties of the ACM were evaluated. The half-life time (defined as the time taken for the foam to collapse to half of its initial volume) of foams stabilised by ACM prepared at various temperatures is shown in Fig. 7. Foams stabilised by ACM prepared at 5 °C had a half-life time of 14.5 ± 3.0 min. Those stabilised by ACM prepared at 37 °C demonstrated similar stability, with a half-life time of 12.9 ± 3.5 min. A marked increase in foam stability was observed for ACM prepared at 65 °C, as evident from a tripling of the half-life time (Fig. 7).

5. Discussion

5.1. Effect of the preparation temperature on micelle structure and composition

The results show that the temperature during preparation has irreversible effects on the composition and structure of the ACM. The fractions of micellar calcium, phosphate, and especially magnesium were permanently increased when ACM were prepared at higher temperatures (Fig. 1) and this was accompanied by an increase in the size of the nanoclusters (Table 3). Heating pre-formed casein micelles has a similar effect on the partitioning of ions between the micellar phase and serum phase because the solubility of calcium phosphate decreases with temperature (Van Kemenade and De Bruyn, 1987), but these increases are almost fully reversible (Pouliot et al., 1989b) and re-equilibration occurs rapidly (i.e. within minutes; Liu et al., 2013). In this study, the ACM were stored for at least 24 h at the same temperature before analysis, during which the ions would have had ample time to re-equilibrate. However, this did not occur, suggesting that the preparation temperature has a lasting effect on the partitioning of ions.

This finding complements the results of a recent study that showed that changing the pH during preparation has a markedly different effect on the micellar calcium phosphate than adjusting the pH to that same value after preparation (Fan et al., 2024). An explanation for this is that colloidal calcium phosphate is not in complete dynamic equilibrium with soluble calcium and phosphate. This is also reflected in the findings that 25 to 40 % of the colloidal calcium and phosphate in bovine milk or artificial casein micelles cannot be exchanged with ions in the serum (Pierre et al., 1983; Yamauchi et al., 1969; Zhang et al., 1996; Zhang and Aoki, 1996). It could be that the binding of caseins to calcium phosphate nanoclusters effectively 'seals' the nanoclusters and prevents the exchange of ions between the nanoclusters and the serum. The binding of caseins to the nanoclusters in itself seems permanent as long as the

integrity of the nanoclusters is maintained (Rose, 1968). An alternative hypothesis could be that an increased temperature during preparation causes the irreversible formation of crystalline calcium phosphate phases instead of only amorphous calcium phosphate nanoclusters, but our data do not allow for confirmation of this hypothesis.

The preparation temperature also permanently affected the assembly of the caseins into the ACM. The caseins were most efficiently assembled into casein micelles at the temperature of the mammary gland (about 37 °C), whereas both decreasing and increasing the preparation temperature resulted in casein aggregation, especially at the high temperature of 65 °C (Fig. 2). The aggregated casein was presumably present in the form of aggregates of partially-formed casein micelles, which would also include part of the colloidal ions. The structure of the ACM densified at higher preparation temperatures, as evident from the increased mass of the protein heterogeneities in the micelle interior and the increased average mass of a micelle (Table 3) while the overall size (Fig. 3) and hydration (Fig. 5) of the ACM decreased. Moreover, the fraction of serum casein (especially β- and κ-casein) increased with a higher preparation temperature from 37 to 65 °C (Fig. 2). Anema and Klostermeyer (1997) observed casein dissociation when natural casein micelles were heated (30–70 °C) at pH ≥ 6.7 and found that this was not reversible upon cooling back to room temperature. Similar to our results, this effect was most prominent for κ-casein, but the process by which casein is dissociated from micelles remains unclear. It is unlikely that this is related to hydrophobic interactions since these would increase rather than decrease in strength with increasing temperature and would be reversible upon cooling. Instead, the slight decrease in the fraction of soluble calcium (Fig. 1A) and the resulting increase in the solvent quality of the serum for caseins may partially explain the increased levels of serum casein. Anema and Klostermeyer (1997) related the dissociation of caseins from micelles to the conversion of the native form of colloidal, amorphous calcium phosphate to an alternative form that is less capable of maintaining micellar integrity. We concur that this is a likely candidate to cause permanent casein dissociation from the ACM, but further research is needed to positively identify the mechanism behind this.

The extensive aggregation of casein micelles at 65 °C is also difficult to explain. If the aggregation were governed by interactions through which caseins generally interact with each other (i.e. hydrophobic interactions, electrostatic interactions, hydrogen bonding, bridging interactions), it would be expected that aggregation *during* ACM formation would be reverted *after* preparation due to the reversibility of these non-covalent interactions. The observed aggregation must therefore be governed by more permanent interactions. Disulphide bonding could be an explanation for the aggregation at 65 °C since disulphide exchange interactions are promoted at increased temperatures. Both α_{s2}-casein and κ-casein contain two cysteine residues and could therefore have aggregated, at least to a limited extent, through disulphide bonding. Another explanation could be the decreased propensity of κ-casein to assemble into micelles at higher temperatures, by which incompletely stabilised ACM were formed that subsequently formed larger aggregates. However, the mechanism responsible for this aggregation of casein micelles at low and high temperatures should be the subject of future research to yield a conclusive answer, and also to explain the limited aggregation observed at a preparation temperature of 5 °C (Fig. 2).

The size of the ACM, however, was minimally affected by these changes in micellar structure, showing only a slight decrease in the studied temperature range (Fig. 3). This aligns well with studies that concluded that micellar size is independent of temperature (Ono et al., 1990; Takagi et al., 2022, 2023). Moreover, studies that subjected pre-formed casein micelles to a heat treatment (in the absence of whey proteins) and then measured their size after cooling down to room temperature found that micelle size increases with increasing heating temperature due to casein micelle aggregation (Fan et al., 2024; Wang and Ma, 2020). In our experiments, the ACM were *prepared* at various temperatures but *analysed* at a fixed temperature after removal of the aggregates by filtration. It is therefore reasonable that we find a relatively stable micellar size at higher preparation temperatures (Fig. 3). The minor decrease at higher temperatures may be explained by the densification of the protein network. The reason for the peak in micelle size at a preparation temperature of 37 °C remains unclear, but this may be related to the fraction of micellar casein that was highest in this mixture (Fig. 2).

Keeping in mind that one is a mode and the other an average, combination of R_g and R_h allows calculation of the shape factor R_g/R_h. This factor was approximately unity (0.98–1.01) for ACM prepared between 5 and 37 °C and around 0.9 for ACM prepared at 50 and 65 °C. Factors of this order of magnitude describe spherical particles and have previously been found for cross-linked casein aggregates (Abbate et al., 2019; Abdelmohsen et al., 2016; Siirilä et al., 2019).

5.2. Effect of the preparation temperature on functional properties

The functional properties of the ACM were significantly affected by the preparation temperature. The differences in coagulation behaviour are likely related to the variations in the fraction of micellar casein. ACM prepared at 25 and 37 °C exhibited the highest fraction of micellar casein (Fig. 2) and produced the firmest curds upon coagulation (Fig. 6). ACM prepared at 5 °C exhibited a lower fraction of micellar casein due to the increased casein aggregation (Fig. 2). These aggregates likely contribute little to the strength of the gel network formed upon renneting, resulting in weaker curds (Fig. 6). At higher preparation temperatures the fraction of micellar casein decreased significantly (Fig. 2), leading to a sharp decline in curd firmness (Fig. 6). The decrease in the concentration of soluble calcium (Fig. 1A) may have had an additional effect on the coagulation behaviour of these ACM. Serum calcium facilitates micelle-micelle interactions that lead to the formation of a gel network. Reduced serum calcium levels prolong the coagulation time and decrease the final gel firmness (Dalgleish, 1983; Sandra et al., 2012; Udabage et al., 2001). Although the decrease in serum calcium was modest, this effect may have been amplified by the pH adjustment prior to coagulation, further reducing the curd firmness of ACM prepared at higher temperatures.

Foam stability, on the other hand, was primarily influenced by the level of serum casein and the extent of casein micelle aggregation. Serum caseins dominate the properties of air-water interfaces, whereas casein micelles contribute minimally to the stabilisation of these interfaces (Zhou et al., 2022). Additionally, large casein micelle aggregates (> 5 μm) enhance foam stability as they get trapped in the foam lamellae and slow the drainage of liquid from the foam (Chen et al., 2017, 2018). Similar stabilising effects have been observed with other particles, such as protein-polyphenol complexes (Yang et al., 2021). For ACM prepared between 5 and 37 °C, the fraction of serum casein remained relatively constant, while the extent of casein aggregation decreased (Fig. 2). This explains the observed decrease in foam stability as the preparation temperature increased from 5 to 37 °C (Fig. 7). In contrast, for mixtures prepared at temperatures above 37 °C, both the serum casein concentration and the level of casein aggregation increased (Fig. 2). This all results in a marked increase in foam stability, as evidenced by the enhanced half-life times (Fig. 7).

6. Conclusions

The temperature during preparation of artificial casein micelles (ACM) has significant and irreversible effects on their composition, structure, and functionality. As the preparation temperature increases, the fraction of micellar calcium phosphate and magnesium, along with the size of calcium phosphate nanoclusters and the fraction of serum casein, increases, while the hydration and overall size of the ACM decreases. The micelle structure thereby densifies with a higher preparation temperature.

Extensive casein micelle aggregation occurred at both 5 °C and, more notably, 65 °C. ACM prepared at intermediate temperatures, particularly 25 and 37 °C, exhibited the highest fraction of micellar casein, producing the firmest curds upon chymosin-induced coagulation. By contrast, the increased fraction of serum casein and the presence of casein aggregates at higher and lower preparation temperatures enhanced the foaming properties.

These findings demonstrate that the temperature during micelle formation is a critical parameter in micelle assembly and the partitioning of casein and salts between the micellar and serum phases, which, in turn, affects their functional properties. While further research is required to elucidate the underlying phenomena, this research highlights the possibility of tailoring the properties and functionality of ACM to specific applications by controlling the preparation temperature.

CRediT authorship contribution statement

Laurens J. Antuma: Writing – original draft, Methodology, Investigation, Formal analysis, Conceptualization. **Yuxuan Si:** Investigation. **Vasil M. Garamus:** Methodology, Investigation, Formal analysis. **Jan Skov Pedersen:** Writing – original draft, Formal analysis. **Volker Gräf:** Writing – review & editing, Methodology, Formal analysis. **Elke Walz:** Writing – review & editing, Methodology, Formal analysis. **Remko M. Boom:** Writing – review & editing, Supervision, Funding acquisition, Conceptualization. **Julia K. Keppler:** Writing – review & editing, Supervision, Funding acquisition, Conceptualization.

Declaration of competing interest

The authors declare that they have no known competing financial interests or personal relationships that could have appeared to influence the work reported in this research.

Acknowledgements

The work for this publication has been undertaken as part of the GOUDA project, which has received funding from the European Union's Horizon 2020 research and innovation programme through Eurostars (E! 114377). The authors would like to thank Mr. Christian Geuter and Ms. Jasmin Klein from the Max Rubner-Institut (MRI) for their excellent technical support and assistance with the dynamic light scattering and AF4 measurements. Sasja van den Akker is thanked for her execution of preliminary experiments.

Data availability

Data will be made available on request.

References

Abbate, R.A., Raak, N., Boye, S., Janke, A., Rohm, H., Jaros, D., Lederer, A., 2019. Asymmetric flow field flow fractionation for the investigation of caseins cross-linked by microbial transglutaminase. Food Hydrocoll. 92, 117–124. https://doi.org/10.1016/j.foodhyd.2019.01.043.

Abdelmohsen, L.K.E.A., Rikken, R.S.M., Christianen, P.C.M., van Hest, J.C.M., Wilson, D. A., 2016. Shape characterization of polymersome morphologies *via* light scattering techniques. Polym 107, 445–449. https://doi.org/10.1016/j.polymer.2016.06.067.

Anema, S.G., Klostermeyer, H., 1997. Heat-induced, pH-dependent dissociation of casein micelles on heating reconstituted skim milk at temperatures below 100°C. J. Agric. Food Chem. 45 (4), 1108–1115. https://doi.org/10.1021/jf960507m.

Antuma, L.J., Braitmaier, S.H., Garamus, V.M., Hinrichs, J., Boom, R.M., Keppler, J.K., 2024a. Engineering artificial casein micelles for future food: preparation rate and coagulation properties. J. Food Eng. 366, 111868. https://doi.org/10.1016/j.jfoodeng.2023.111868.

Antuma, L.J., Stadler, M., Garamus, V.M., Boom, R.M., Keppler, J.K., 2024b. Casein micelle formation as a calcium phosphate phase separation process: preparation of artificial casein micelles through vacuum evaporation and membrane processes. Innov. Food Sci. Emerg. Technol. 92, 103582. https://doi.org/10.1016/j.ifset.2024.103582.

Antuma, L.J., Steiner, I., Garamus, V.M., Boom, R.M., Keppler, J.K., 2023. Engineering artificial casein micelles for future food: is casein phosphorylation necessary? Food Res. Int. 173, 113315. https://doi.org/10.1016/j.foodres.2023.113315.

Barker, J.G., Pedersen, J.S., 1995. Instrumental smearing effects in radially symmetric small-angle neutron scattering by numerical and analytical methods. J. Appl. Crystallogr. 28 (2), 105–114. https://doi.org/10.1107/S0021889894010095.

Chen, M., Feijen, S., Sala, G., Meinders, M.B.J., van Valenberg, H.J.F., van Hooijdonk, A. C.M., van der Linden, E., 2018. Foam stabilized by large casein micelle aggregates: the effect of aggregate number in foam lamella. Food Hydrocoll. 74, 342–348. https://doi.org/10.1016/j.foodhyd.2017.08.026.

Chen, M., Sala, G., Meinders, M.B.J., van Valenberg, H.J.F., van der Linden, E., Sagis, L. M.C., 2017. Interfacial properties, thin film stability and foam stability of casein micelle dispersions. Colloids Surf. B 149, 56–63. https://doi.org/10.1016/j.colsurfb.2016.10.010.

Creamer, L.K., Berry, G.P., Mills, O.E., 1977. A study of the dissociation of β-casein from the bovine casein micelle at low temperature. N. Z. J. Dairy Sci. Technol. 12, 58–66.

Dalgleish, D.G., 1983. Coagulation of renneted bovine casein micelles: dependence on temperature, calcium ion concentration and ionic strength. J. Dairy Res. 50 (3), 331–340. https://doi.org/10.1017/S0022029900023165.

Davies, D.T., Law, A.J.R., 1983. Variation in the protein composition of bovine casein micelles and serum casein in relation to micellar size and milk temperature. J. Dairy Res. 50 (1), 67–75. https://doi.org/10.1017/S0022029900032532.

Davies, D.T., White, J.C.D., 1960. The use of ultrafiltration and dialysis in isolating the aqueous phase of milk and in determining the partition of milk constituents between the aqueous and disperse phases. J. Dairy Res. 27 (2), 171–190. https://doi.org/10.1017/S0022029900010256.

Dumpler, J., Kieferle, I., Wohlschläger, H., Kulozik, U., 2017. Milk ultrafiltrate analysis by ion chromatography and calcium activity for SMUF preparation for different scientific purposes and prediction of its supersaturation. Int. Dairy J. 68, 60–69. https://doi.org/10.1016/j.idairyj.2016.12.009.

Fan, Z., Fehér, B., Hettinga, K., Voets, I.K., Bijl, E., 2024. Effect of temperature, pH and calcium phosphate concentration on the properties of reassembled casein micelles. Food Hydrocoll. 149, 109592. https://doi.org/10.1016/j.foodhyd.2023.109592.

Glantz, M., Håkansson, A., Lindmark-Månsson, H., Paulsson, M., Nilsson, L., 2010. Revealing the size, conformation, and shape of casein micelles and aggregates with asymmetrical flow field-flow fractionation and multiangle light scattering. Langmuir 26 (15), 12585–12591. https://doi.org/10.1021/la101892x.

Griffin, M.C.A., Griffin, W.G., 1985. A simple turbidimetric method for the determination of the refractive index of large colloidal particles applied to casein micelles. J. Colloid Interface Sci. 104 (2), 409–415. https://doi.org/10.1016/0021-9797(85)90049-9.

Guimarães, B.O., Gremmen, P., Wijffels, R.H., Barbosa, M.J., D'Adamo, S., 2021. Effect of ammonium formate washing on the elemental composition determination in *Nannochloropsis oceanica*. Aquaculture 538, 736526. https://doi.org/10.1016/j.aquaculture.2021.736526.

Holt, C., Carver, J.A., 2022. Quantitative multivalent binding model of the structure, size distribution and composition of the casein micelles of cow milk. Int. Dairy J. 126, 105292. https://doi.org/10.1016/j.idairyj.2021.105292.

Hoppenreijs, L.J.G., Brune, S.E., Biedendieck, R., Krull, R., Boom, R.M., Keppler, J.K., 2024. Exploring functionality gain for (recombinant) β-lactoglobulin through production and processing interventions. Food Bioprocess Technol 17, 4897–4914. https://doi.org/10.1007/s11947-024-03414-z.

Horne, D.S., 2020. Casein micelle structure and stability. In: Boland, M., Singh, S. (Eds.), Milk proteins: from expression to food. Elsevier, pp. 213–250.

Lie-Piang, A., Leeman, M., Castro, A., Börjesson, E., Nilsson, L., 2021. Revisiting the dynamics of proteins during milk powder hydration using asymmetric flow field-flow fractionation (AF4). Curr. Res. Food Sci. 4, 83–92. https://doi.org/10.1016/j.crfs.2021.02.004.

Liu, D.Z., Weeks, M.G., Dunstan, D.E., Martin, G.J.O., 2013. Temperature-dependent dynamics of bovine casein micelles in the range 10–40°C. Food Chem. 141 (4), 4081–4086. https://doi.org/10.1016/j.foodchem.2013.06.130.

Moitzi, C., Portnaya, I., Glatter, O., Ramon, O., Danino, D., 2008. Effect of temperature on self-assembly of bovine β-casein above and below isoelectric pH. Structural analysis by cryogenic-transmission electron microscopy and small-angle X-ray scattering. Langmuir 24 (7), 3020–3029. https://doi.org/10.1021/la702802a.

Nöbel, S., Kern, C., Sonne, A., Bähler, B.M., Hinrichs, J., 2016. Apparent voluminosity of casein micelles in the temperature range 35–70°C. Int. Dairy J. 59, 80–84. https://doi.org/10.1016/j.idairyj.2016.03.010.

Nöbel, S., Weidendorfer, K., Hinrichs, J., 2012. Apparent voluminosity of casein micelles determined by rheometry. J. Colloid Interface Sci. 386 (1), 174–180. https://doi.org/10.1016/j.jcis.2012.07.075.

O'Connell, J.E., Fox, P.F., 2003. Heat-induced coagulation of milk. Fox, P.F., McSweeney, P.L.H.. In: Advanced dairy chemistry, 1. Proteins. Springer US, pp. 879–945.

Ono, T., Murayama, T., Kaketa, S., Odagiri, S., 1990. Changes in the protein composition and size distribution of bovine casein micelles induced by cooling. Agricult. Biol. Chem. 54 (6), 1385–1392. https://doi.org/10.1080/00021369.1990.10870165.

Pedersen, J.S., 1994. Determination of size distribution from small-angle scattering data for systems with effective hard-sphere interactions. J. Appl. Crystallogr. 27 (4), 595–608. https://doi.org/10.1107/S0021889893013810.

Pedersen, J.S., 1997. Analysis of small-angle scattering data from colloids and polymer solutions: modeling and least-squares fitting. Adv. Colloid Interface Sci 70 (1–3), 171–210. https://doi.org/10.1016/S0001-8686(97)00312-6.

Pedersen, J.S., Møller, T.L., Raak, N., Corredig, M., 2022. A model on an absolute scale for the small-angle X-ray scattering from bovine casein micelles. Soft Matter 18 (45), 8613–8625. https://doi.org/10.1039/D2SM00724J.

Pedersen, J.S., Posselt, D., Mortensen, K., 1990. Analytical treatment of the resolution function for small-angle scattering. J. Appl. Crystallogr. 23 (4), 321–333. https://doi.org/10.1107/S0021889890003946.

Pierre, A., Brulé, G., 1981. Mineral and protein equilibria between the colloidal and soluble phases of milk at low temperature. J. Dairy Res. 48 (3), 417–428. https://doi.org/10.1017/S0022029900021890.

Pierre, A., Brulé, G., Fauquant, J., 1983. Etude de la mobilité du calcium dans le lait à l'aide du calcium 45. Lait 63 (633–634), 473–489. https://doi.org/10.1051/lait:1983633-63430.

Pouliot, Y., Boulet, M., Paquin, P., 1989a. Observations on the heat-induced salt balance changes in milk I. Effect of heating time between 4 and 90 °C. J. Dairy Res. 56 (2), 185–192. https://doi.org/10.1017/S0022029900026406.

Pouliot, Y., Boulet, M., Paquin, P., 1989b. Observations on the heat-induced salt balance changes in milk II. Reversibility on cooling. J. Dairy Res. 56 (2), 193–199. https://doi.org/10.1017/S0022029900026418.

Rose, D., 1968. Relation between micellar and serum casein in bovine milk. J. Dairy Sci. 51 (12), 1897–1902. https://doi.org/10.3168/jds.S0022-0302(68)87308-4.

Rose, D., Tessier, H., 1959. Composition of ultrafiltrates from milk heated at 80 to 230°F. in relation to heat stability. J. Dairy Sci. 42 (6), 969–980. https://doi.org/10.3168/jds.S0022-0302(59)90680-0.

Sandra, S., Ho, M., Alexander, M., Corredig, M., 2012. Effect of soluble calcium on the renneting properties of casein micelles as measured by rheology and diffusing wave spectroscopy. J. Dairy Sci. 95 (1), 75–82. https://doi.org/10.3168/jds.2011-4713.

Schmidt, D.G., Both, P., Koops, J., 1979. Properties of artificial casein micelles. 3. Relationship between salt composition, size and stability towards ethanol, dialysis and heat. Neth. Milk Dairy J. 33, 40–48.

Schmidt, D.G., Koops, J., 1977. Properties of artificial casein micelles. 2. Stability towards ethanol, dialysis, pressure and heat in relation to casein composition. Neth. Milk Dairy J. 31 (4), 342–351.

Schmidt, D.G., Koops, J., Westerbeek, D., 1977. Properties of artificial casein micelles. 1. Preparation, size distribution and composition. Neth. Milk Dairy J. 31 (4), 328–341.

Siirilä, J., Häkkinen, S., Tenhu, H., 2019. The emulsion polymerization induced self-assembly of a thermoresponsive polymer poly(*N-vinylcaprolactam*). Polymer Chem. 10 (6), 766–775. https://doi.org/10.1039/C8PY01421C.

Takagi, H., Nakano, T., Aoki, T., Tanimoto, M., 2022. Temperature dependence of the casein micelle structure in the range of 10–40°C: an *in-situ* SAXS study. Food Chem. 393, 133389. https://doi.org/10.1016/j.foodchem.2022.133389.

Takagi, H., Nakano, T., Aoki, T., Tanimoto, M., 2023. The structural changes of a bovine casein micelle during temperature change; in situ observation over a wide spatial scale from nano to micrometer. Soft Matter 19 (24), 4562–4570. https://doi.org/10.1039/D3SM00146F.

Udabage, P., McKinnon, I.R., Augustin, M.A., 2001. Effects of mineral salts and calcium chelating agents on the gelation of renneted skim milk. J. Dairy Sci. 84 (7), 1569–1575. https://doi.org/10.3168/jds.S0022-0302(01)74589-4.

van Kemenade, M.J.J.M., de Bruyn, P.L., 1987. A kinetic study of precipitation from supersaturated calcium phosphate solutions. J. Colloid Interface Sci. 118 (2), 564–585. https://doi.org/10.1016/0021-9797(87)90490-5.

Wang, Q., Ma, Y., 2020. Effect of temperature and pH on salts equilibria and calcium phosphate in bovine milk. Int. Dairy J. 110, 104713. https://doi.org/10.1016/j.idairyj.2020.104713.

Yamauchi, K., Yoneda, Y., Koga, Y., Tsugo, T., 1969. Exchangeability of colloidal calcium in milk with soluble calcium. Agric. Biol. Chem. 33 (6), 907–914. https://doi.org/10.1080/00021369.1969.10859396.

Yang, J., Lamochi Roozalipour, S.P., Berton-Carabin, C.C., Nikiforidis, C.V., van der Linden, E., Sagis, L.M.C., 2021. Air-water interfacial and foaming properties of whey protein - sinapic acid mixtures. Food Hydrocoll. 112, 106467. https://doi.org/10.1016/j.foodhyd.2020.106467.

Zhang, Z.P., Aoki, T., 1996. Behaviour of calcium and phosphate in bovine casein micelles. Int. Dairy J. 6 (8–9), 769–780. https://doi.org/10.1016/0958-6946(96)00006-4.

Zhang, Z.P., Fujii, M., Aoki, T., 1996. Behavior of calcium and phosphate in artificial casein micelles. J. Dairy Sci. 79 (10), 1722–1727. https://doi.org/10.3168/jds.S0022-0302(96)76538-4.

Zhou, X., Yang, J., Sala, G., Sagis, L.M.C., 2022. Are micelles actually at the interface in micellar casein stabilized foam and emulsions? Food Hydrocoll. 129, 107610 https://doi.org/10.1016/j.foodhyd.2022.107610.